

AD-A138 924

WAVE ATTENUATION IN PERIODIC STRUCTURES(U) MINNESOTA
UNIV MINNEAPOLIS DEPT OF AEROSPACE ENGINEERING AND
MECHANICS R PLUNKETT ET AL. 09 FEB 84 AEM-RP-84-1

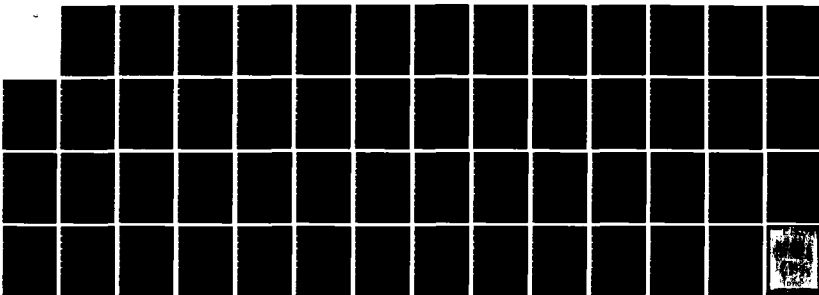
1/1

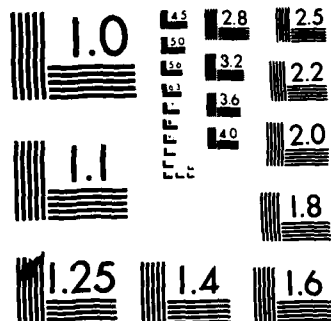
UNCLASSIFIED

N80014-82-K-0591

F/G 20/11

NL





MICROCOPY RESOLUTION TEST CHART
NATIONAL BUREAU OF STANDARDS-1963-A

2

REPORT DOCUMENTATION PAGE

READ INSTRUCTIONS
BEFORE COMPLETING FORM

1. REPORT NUMBER AEM-RP-84-1 ✓		2. GOVT ACCESSION NO.	3. RECIPIENT'S CATALOG NUMBER
4. TITLE (and Subtitle) Attenuation of Bending Waves in Periodic Structures		5. TYPE OF REPORT & PERIOD COVERED Interim Report 7/83 - 1/84	
7. AUTHOR(s) Robert Plunkett Ajit K. Roy		6. PERFORMING ORG. REPORT NUMBER	
8. PERFORMING ORGANIZATION NAME AND ADDRESS Dept. Aero Eng. & Mech. University of Minnesota Minneapolis, MN 55455		9. CONTRACT OR GRANT NUMBER(s) N00014-82-K-0591	
11. CONTROLLING OFFICE NAME AND ADDRESS Organizational Effectiveness Group Office of Naval Research (Code 4420E) Arlington, VA 22217		10. PROGRAM ELEMENT, PROJECT, TASK AREA & WORK UNIT NUMBERS	
14. MONITORING AGENCY NAME & ADDRESS (if different from Controlling Office) Office of Naval Research (Code 432) Dr. N. L. Basdekas Arlington, VA 22217		12. REPORT DATE Feb. 9, 1984	
		13. NUMBER OF PAGES 51	
		15. SECURITY CLASS. (of this report) Unclassified	
		15a. DECLASSIFICATION/DOWNGRADING SCHEDULE	

16. DISTRIBUTION STATEMENT (of this Report)
Approved for public release; distribution unlimited

17. DISTRIBUTION STATEMENT (of the abstract entered in Block 20, if different from Report)

18. SUPPLEMENTARY NOTES

19. KEY WORDS (Continue on reverse side if necessary and identify by block number)
Traveling Waves, Periodic Structures
Wave Attenuation, Vibration Control

DTIC
COPY
15 1984
E

20. ABSTRACT (Continue on reverse side if necessary and identify by block number)
The analytical and experimental results for the attenuation of traveling bending waves in a uniform beam with tuned periodic cantilever ribs are presented. Results are given for one, three, five, seven, fifteen and an infinite number of sections.

AD A138924

DTIC FILE COPY

84 03 13 059

ABSTRACT

The analytical and experimental results for traveling bending waves in a uniform beam with tuned periodic cantilever ribs are presented in this report. Two analytical models were developed: one, is for an infinite array of periodic sections and the other is for a finite array of periodic sections in an infinite beam. Several types of periodic sections were considered. The bending moment spectrum was measured for a traveling wave in a uniform beam caused by impact. The insertion loss as a function of frequency was measured for such a beam with 1,3,5,7 and 15 sets of symmetric sections. There is good agreement between the computed bending moment spectra and the measured ones for all sets of cantilevers considered. The width of attenuation bands increased with an increasing number of cantilever sets, and the spectrum for 15 cantilever sets was a close approximation to that of the computed spectrum for an infinite number.

1. INTRODUCTION

The theory of wave propagation in periodic structures has been developed by solid state physicists and electrical engineers for some time [1,2]. The application of this theory to predicting vibration responses of periodic engineering structures due to broad band pressure fluctuation is relatively recent and has been applied, primarily, to the analysis of periodic structures as band pass filters for bending waves [3,4,5,6]. The analysis for an infinite ribbed bar has been published with some limited confirming evidence [7]. The objective of this study is to get extensive quantitative results, both analytical and experimental, for a beam with tuned periodic cantilever ribs. Two analytical models are presented for such a periodic structure in which the periodic sections consist of constant cross-section rectangular beam elements. One of the models is for an infinite array of periodic sections and the other is for a finite array of periodic sections in an infinite beam. The attenuation in the infinite model is either zero or infinite; the stop and pass bands are conveniently found by an eigenvalue technique. The actual value of the attenuation must be found for a finite model and so an impedance technique is used. Three types of periodic sections are considered, symmetric (two sided cantilevers), asymmetric (one sided) and antisymmetric (alternately on each side). The impedance model is

sufficiently versatile to predict the response of ordered as well as disordered periodic sections with no limitations on the number of such sections. This report gives experimental and analytical results for an ordered periodic beam with symmetric sections of 1, 3, 5, 7 and 15 sets of cantilevers.

In an earlier report [8] the analytical model for the infinite periodic beam with symmetric sections was developed and compared with measured results. This work is briefly reviewed in Section 2.3 of this report.

In this report, Section 2 gives the analysis, Section 3 describes the experimental method, Section 4 contains the results and Section 5 discusses the comparison of the experimental and analytical results.

2. ANALYSIS

2.1 GEOMETRY

Our periodic structure consists of an array of periodic sections. Elements of the periodic section are uniform beams of rectangular cross-section. Three section types are considered:

a) Symmetric: Sections of this type consist of a uniform beam element with a double cantilever element attached to it at its right end, figure A.1.

b) Asymmetric: Sections of this type consist of a uniform beam element with a cantilever attached to one side at the right end, figure A.2.

c) Antisymmetric: Sections of this type consist of a uniform beam element with cantilever elements attached alternately on each side, one at the center and the other at the right end, figure A.3.

2.2 EQUATIONS OF MOTION

In first order theory, the differential equation for the propagation of an extensional wave in a uniform beam is:

$$EA \frac{\partial^2 u}{\partial x^2} + \rho A \frac{\partial^2 u}{\partial t^2} = 0 \quad (2.2.1)$$

and that for a bending wave (Bernoulli-Euler) is:

$$D \frac{\partial^4 y}{\partial x^4} + \rho A \frac{\partial^2 y}{\partial t^2} = 0 \quad (2.2.2)$$

If we assume a sinusoidal wave of frequency ω travelling to the right

$$u(x,t) = u(x) \exp(-j\omega t) \quad (2.2.3)$$

$$y(x,t) = v(x) \exp(-j\omega t)$$

where $j = \sqrt{-1}$

the general solutions of equations (2.2.1) and (2.2.2) for a uniform beam are

$$u(x) = E_1 \cos \gamma x + E_2 \sin \gamma x \quad (2.2.4)$$

$$v(x) = A_1 \cosh \beta x + A_2 \sinh \beta x + A_3 \cos \beta x + A_4 \sin \beta x$$

where $\gamma = \omega / c_r$

$c_r = \sqrt{E/\rho}$ is the rod phase velocity

$$\beta^4 = 12 \rho \omega^2 / Et$$

t = beam thickness for a rectangular cross-section

$D = EI$ is the bending stiffness*.

A_1, A_2, A_3, A_4, E_1 and E_2 are constants to be determined from the end boundary conditions.

We can analyse a travelling wave in a periodic structure by using the nodal boundary conditions at the ends of the periodic sections.

2.3 TRANSFER MATRIX

We define a vector composed of six components of

* the anticlastic curvature restraint is not effective for a thin rectangular cross-section at small bending strains and so the $1-\nu^2$ term is omitted.

displacements and forces at a node i

$$Z_i = \begin{Bmatrix} z_{1i} \\ \text{---} \\ z_{2i} \end{Bmatrix} = \begin{Bmatrix} u_i \\ P_i / \gamma EA \\ \text{---} \\ v_i \\ \theta_i / \beta \\ M_i / EI \beta^2 \\ -F_i / EI \beta^3 \end{Bmatrix} \quad (2.3.1)$$

where the components are defined in appendix E and figure 2.2.1.

The elements of the vector Z_i are multiplied by suitable factors to give each the dimension of length. We can find the above vector at the end of a section in terms of the that at the other (figure A.1, A.2 or A.3):

$$Z_i = [H_m]_i Z_{i-1} \quad (2.3.2)$$

$[H_m]_i$ is a (6x6) matrix and is the transfer matrix for the section i , between nodes $(i-1)$ and i of section type m ($m=1,2,3$). We partition the matrix $[H_m]_i$ to get

$$\begin{Bmatrix} z_{1i} \\ \text{---} \\ z_{2i} \end{Bmatrix} = \begin{vmatrix} H_{1m} & H_{2m} \\ \text{---} & \text{---} \\ H_{3m} & H_{4m} \end{vmatrix} \begin{Bmatrix} z_{1(i-1)} \\ \text{---} \\ z_{2(i-1)} \end{Bmatrix}$$

where H_{1m} (2x2) and H_{4m} (4x4) are due to the axial and bending modes alone and H_{2m} (2x4) and H_{3m} (4x2) are the matrices coupling the two modes of vibration. The transfer matrices $[H_m]_i$ for each type of section are given in appendix A.

2.4 EIGENVALUE MODEL

The periodic beam is considered to have an infinite array of identical periodic sections. If we have a wave of frequency ω traveling in an undistorted fashion, it must attenuate by the same fraction in each section. Thus we may write

$$z_i = \lambda_m z_{i-1} \quad (2.4.1)$$

where λ_m is the ratio between successive periodic repeats. From equation (2.3.2) we have

$$z_i = [H_m] z_{i-1} = \lambda_m z_{i-1} \quad (2.4.2)$$

This is an eigenvalue problem where $[H_m]$ is a function of frequency*. Since all of the sections are identical, the

* submatrices G and F of $[H_m]_i$ were incorrectly reported in reference [8]. The corrected version is given in equation (E.2) and (E.7), appendix E.

subscript i of the transfer matrix is dropped. There are six roots to the eigenvalue problem which are, in general, complex. It can be shown that the absolute values are equal to or less than one. If the value is one, the magnitude of the travelling wave is unattenuated; if it is less than one, it must eventually die out. The stop and pass bands calculated for $h/L = 0.48$ are shown in figure 4.1.1 and the predicted results are compared with measured ones in figure 4.1.2 which is discussed in section 4.

2.5 IMPEDANCE MODEL

The structure is modeled in three parts. The middle part of the structure consists of a finite array of a number of periodic sections; the two end parts are semi-infinite uniform beams attached to the middle part. Since the experimental portion of this project considers the response of the beam to the impulsive force applied transversely near the center, the Sommerfeld condition requires us to consider only waves travelling to the right at the right end and to the left at the left end.

2.6 IMPEDANCE MATRIX and INSERTION LOSS

The impedance matrix Q_i^\pm relates the force vector, N_i , at a node to the displacement vector, W_i , at that node (figure 2.6.1). The sign used as the superscript on the impedance matrix signifies the direction in which one looks.

$$N_i = Q_i^+ W_i$$

Where

$$N_i = \begin{Bmatrix} M_i / EI \beta^2 \\ -F_i / EI \beta^3 \\ P_i / \gamma EA \end{Bmatrix}$$

$$W_i = \begin{Bmatrix} v_i \\ \theta_i / \beta \\ u_i \end{Bmatrix}$$

We now rearrange the vector Z_i , for convenience, as

$$\hat{Z}_i = \begin{Bmatrix} W_i \\ \text{---} \\ N_i \end{Bmatrix} \quad (2.6.1a)$$

The impedance matrix at node n which is the first node of the right hand semi-infinite uniform beam (figure 2.6.1) is (appendix B equation (B.1)):

$$Q_n^+ = \begin{vmatrix} -j & -(1+j) & 0 \\ -(1-j) & j & 0 \\ 0 & 0 & j \end{vmatrix}; \quad j = \sqrt{-1} \quad (2.6.1b)$$

$$N_n = Q_n^+ W_n$$

The transfer impedance matrix, $[R_{on}^+]_m$ gives the force vector at the n'th node in terms of the displacement vector at the 0'th node:

$$N_n = [R_{on}^+]_m W_0 \quad (2.6.2)$$

It is shown in appendix C that $[R_{on}^+]_m$ can be computed from K_m , the inverse of the transfer matrix:

$$[R_{on}^+]_m = Q_n^+ \left[\{K_{m1}\}_n + \{K_{m2}\}_n Q_n^+ \right]^{-1} \left[\{K_{m1}\}_{n-1} + \{K_{m2}\}_{n-1} Q_{n-1}^+ \right]^{-1} \dots \dots \dots \left[\{K_{m1}\}_2 + \{K_{m2}\}_2 Q_2^+ \right]^{-1} \left[\{K_{m1}\}_1 + \{K_{m2}\}_1 Q_1^+ \right]^{-1} \quad (2.6.3)$$

A bending wave traveling to the right in a bar will split into a reflected wave and a transmitted wave at a change of cross section which occurs at a node. Therefore at the zero'th node

$$\begin{Bmatrix} v_I \\ \theta_I/\beta \\ u_I \end{Bmatrix} = \begin{Bmatrix} v_R \\ \theta_R/\beta \\ u_R \end{Bmatrix} + \begin{Bmatrix} v_T \\ \theta_T/\beta \\ u_T \end{Bmatrix}$$

or
$$W_I = W_R + W_T = W_R + W_0 \quad (2.6.4)$$

In the same way for the forces

$$\begin{Bmatrix} M_I \\ F_I \\ P_I \end{Bmatrix} = \begin{Bmatrix} M_R \\ F_R \\ P_R \end{Bmatrix} + \begin{Bmatrix} M_T \\ F_T \\ P_T \end{Bmatrix}$$

or $N_I = N_R + N_T = N_R + N_O$ (2.6.5)

The relations between force and displacement vectors at node 0 are

$$N_I = [Q_o^+]_I W_I, \quad N_R = [Q_o^+]_R W_R$$
 (2.6.6)

$$N_T = Q_o^+ W_T = Q_o^+ W_O$$

where $W_k = \begin{Bmatrix} v_k \\ \theta_k/\beta \\ u_k \end{Bmatrix}$, $N_k = \begin{Bmatrix} M_k/EI\beta^2 \\ -F_k/EI\beta^3 \\ P_k/\gamma EA \end{Bmatrix}$; (k=I,R,T)

$$[Q_o^+]_I = \begin{vmatrix} -1 & 0 & 0 \\ j & 0 & 0 \\ 0 & 0 & -j \end{vmatrix}$$

$[Q_o^+]_I$ is obtained from equation (D.5), appendix D.

$$[Q_o^+]_R = \begin{vmatrix} -j & (1+j) & 0 \\ 1-j & j & 0 \\ 0 & 0 & j \end{vmatrix}$$

Q_0^+ is obtained from equation (C.4), Appendix C for $i=0$. Since the reflected wave at node zero propagates through the uniform semi-infinite beam in negative x direction, $[Q_0^+]_R$ is obtained in the same way as Q_0^+ is obtained in appendix B but with opposite sign of x .

Using equations (2.6.6) and (2.6.4), equation (2.6.5) can be written

$$N_I = [Q_0^+]_R (W_I - W_0) + N_0$$

$$N_I - [Q_0^+]_R W_I = -[Q_0^+]_R [Q_0^+]^{-1} N_0 + N_0$$

$$\text{or } \{I - [Q_0^+]_R [Q_0^+]^{-1}\} N_I = \{I - [Q_0^+]_R [Q_0^+]^{-1}\} N_0$$

$$N_I = \{I - [Q_0^+]_R [Q_0^+]^{-1}\}^{-1} \{I - [Q_0^+]_R [Q_0^+]^{-1}\} Q_0^+ W_0$$

$$N_I = S W_0$$

$$\text{where } S = \{I - [Q_0^+]_R [Q_0^+]^{-1}\}^{-1} \{I - [Q_0^+]_R [Q_0^+]^{-1}\} Q_0^+$$

$$\text{So that } W_0 = S^{-1} N_I \quad (2.6.7)$$

S is a (3x3) matrix, given in appendix D. Substituting equation (2.6.7) into equation (2.6.2) we obtain,

$$N_n = J_m N_I \quad (2.6.8)$$

where $J_m = [R_{on}^+]_m S^{-1}$

Since bending strains were measured in our experiment we consider the bending moment element of N_n in equation (2.6.8):

$$M_n/EI\beta^2 = J_m(1,1) M_I/EI\beta^2 + J_m(1,2) \cdot -F_I/EI\beta^3 + J_m(1,3) P_I/\gamma EA$$

Substituting the values of M_I , F_I and P_I in terms of the amplitudes of the incident axial and bending waves (equation (D.5) we find that

$$M_n/EI\beta^2 = [-J_m(1,1) + jJ_m(1,2)] V_1 + jJ_m(1,3) U_1 \quad (2.6.9)$$

For the beam with symmetric sections, $J_m(1,3)=0$ so that the bending mode is not coupled with the axial mode.

The dB Insertion Loss (IL) due to the presence of the periodic section is ($m=1$):

$$IL(\omega) = 20 \log_{10} \frac{\|M_I\|}{\|M_n\|} = -20 \log_{10} \left\| J_m(1,1) - jJ_m(1,2) \right\| \quad (2.6.10)$$

We have assumed that the damping dissipation in the uniform beam is negligible so that the spectrum magnitude is the

same everywhere. Spectrum measurements confirm this assumption. Thus the transmitted spectrum, S_p , can be found from the incident spectrum,

$$S_p(\omega) = S_u(\omega) - IL(\omega) \quad (2.6.11)$$

where $S_u(\omega)$ is the uniform beam spectrum.

3.1 INSTRUMENTATION

With one exception, the instrumentation is the same as that described in reference [8], figure 3.1.1. Instead of using the HIPlot X-Y recorder to make hard copies of the signals stored in the spectrum analyzer a HP-85 computer and a HP 7225B plotter were used. This system is more flexible for getting a hard copy of any stored signal.

3.2 BEAM and CANTILEVERS

A uniform steel beam, 0.250 inch thick by 2.00 inch wide and 36 feet long was hung in a horizontal position by 0.030 inch piano wires fastened at 4 feet intervals to the thin edge by welding to 3/4 inch, 6-32 screws in drilled and tapped holes; the screws were locked by locknuts. The wires were fastened to an overhead pipe 4 feet above and adjusted by turnbuckles to equal tension by tuning to the same note. The impact point was 16 feet from one end. The travelling waves were measured at point 10, 10 inches from the impact

point and point 82, 82 inches from the impact point, both on the 20 feet end (figure 3.2.1).

After the uniform beam measurements, 15 pairs of cantilevers each 2.35 inch long were fastened to the beam at 5 inch intervals starting one inch from point 10; the measured resonances of the cantilevers mounted in a short length of beam lay between 1332 and 1386 Hz. The resonant frequency of a 2.35 inch cantilever calculated by using the measured phase velocity is 1394 Hz; if we assume the length (arbitrarily) to be 2.40 inch to account for the elasticity of the base, we get 1340 Hz. The frequencies of waves with wavelengths 10 and 5 inches (5 inches is the distance between two consecutive cantilevers) are respectively 863 and 3452 Hz.

3.3 EXPERIMENTAL TECHNIQUE

3.3.1 FREQUENCY SPAN

Since the bending wave is dispersive with its phase velocity proportional to the square root of its frequency, the low frequency components of the wave take longer to travel from the origin of the wave at the point of impact to a measurement point than do those of higher frequencies. With the finite beam that was used in our experiment, the spectrum of an infinite beam can be obtained if the spectrum is recorded before any reflection from the free

end of the finite beam alters the spectrum; that was achieved with signal travel times appropriate to the frequency span settings of the spectrum analyzer. For a frequency span of 10 kHz (12.5 msec time signal) with 6.5 msec pretrigger time, the total travel time (12.5-6.5 or 6.0 msec) to reach the measurement point 82 (figure 3.2.1) was not enough for waves of frequency 10.4 kHz and lower to return after reflecting from the free end A of the beam. Also it was not enough for frequency 500 Hz and lower to reach the point 82 directly from the impact point. So at this frequency span setting the spectrum between 500 Hz and 10kHz was essentially the same as that of an infinite beam. At the 5 kHz and 2.5 kHz frequency span settings with 25 and 50 msec time signals and 9 and 17.5 msec delay times, travel time for the wave to reach point 82 was respectively (25 - 9 or 16msec) and (50 - 17.5 or 32.5 msec). At these two settings, using the same reasoning, the spectra were good from 63 Hz to 1300 Hz and from 15 Hz to 350 Hz respectively. Thus, to get the spectrum for the infinite beam for the whole frequency range of 10 kHz, spectrum data for frequencies 15 - 320 Hz and 320 - 1480 Hz were taken from the 2.5 kHz and 5 kHz settings respectively and the rest of the spectrum data were taken from the 10 kHz span setting. These three data sets were then combined with appropriate band width corrections.

3.3.2 UNIFORM BEAM

The uniform beam spectrum was measured at point 82. All the measurements were taken with eight averages of the r.m.s. spectrum with gain settings at 10 mV max., and A.C. coupling. The bending moment spectrum is shown in figure 3.3.1.

3.3.3 BEAM WITH CANTILEVERS

The settings of the spectrum analyzer and the pretrigger time were kept the same as in the uniform beam case. The amplitude of the impact was also kept the same to make sure that the incident wave was the same as for the uniform beam. Since the spectrum measured at any point beyond the cantilevers along the uniform (undamped) beam remains the same, all of the measurements of the spectrum were taken at point 82.

4.1 IMPEDANCE MODEL

Equation (2.6.10) was used to calculate the dB Insertion Loss (IL) as a function of frequency for the symmetric periodic case for 1, 3, 5, 7 and 15 pairs of cantilevers. Since the incident wave was assumed to be same with and without the cantilevers the computed spectrum for the periodic beam was calculated from equation (2.6.11) for each number of sets. The computed spectra are compared with the experimental ones in figures 4.2.2a, 4.2.2b, 4.2.2c,

4.2.2d, and 4.2.2e. In some stop bands the computed spectrum values were less than -120 dBV and were below the bottom of the figures.

4.2 EIGENVALUE MODEL

The pass bands and stop bands for an infinite periodic beam calculated by the eigenvalue method reported in [8] are shown in figure 4.1.1. In this model of an infinite number of periodic sections, no attenuation occurs in the pass bands and no transmission occurs in the stop bands. The spectrum computed in this way is compared with the measured spectrum of the periodic beam with fifteen sets of cantilevers in figure 4.1.2.

5. DISCUSSIONS

The agreement between the spectrum computed by the impedance method and the measured spectrum is gratifying for all five cantilever sets considered. The measured attenuation between 6600 Hz and 7300 Hz for 15 sets of cantilevers was much greater than the calculated values. Some indication of this can also be seen in the other figures. The reason for this discrepancy is not known; material damping is much too small to account for it.

Attenuation in the stop bands and the width of the stop bands increased with increasing numbers of cantilever sets.

At fifteen cantilever sets they approximated the computed results for an infinite number. The values of the computed spectrum in most of the stop bands, especially for cantilever pairs five or more, was -250 dBV or below, whereas the experimental attenuation was always less than 35 dBV. This is probably due in part to the 12 bit A/D converter (72 dB full scale) of the spectrum analyzer and in part to leakage caused by the DFT.

APPENDIX A

Transfer Matrices

Considering the axial wave solution of equation (2.2.4) for a uniform beam piece of length L , we obtain (appendix E)

$$Z_{1i} = B Z_{1(i-1)} \quad (\text{A.1})$$

where B is given by equation (E.1) and Z_i is defined in equation (2.3.1). From the bending wave solution, we get (appendix E)

$$Z_{2i} = G Z_{2(i-1)} \quad (\text{A.2})$$

where G is given by equation (E.2).

The process of getting the transfer matrices for any type of periodic sections is similar to that given in section 2.2 of [8] with appropriate equations of equilibrium at a node.

a) Symmetric section ($m=1$)

The equations of equilibrium at node i with the sign conventions shown in figure (A.1) are

$$M_i = M_{1i} - M_{2i} - M_{3i}$$

$$F_i = F_{1i} - P_{2i} + P_{3i}$$

$$P_i = P_{1i} + F_{2i} - F_{3i}$$

Following the same procedure as described in section 2.2 of [8] we obtain the transfer matrix $[H_i]_i$ for this type of section as (equation E.5):

$$[H_i]_i = \begin{vmatrix} H_{11} & H_{21} \\ \text{---} & \text{---} \\ H_{31} & H_{41} \end{vmatrix}_i = \begin{vmatrix} B + D_1 & 0 \\ \text{---} & \text{---} \\ 0 & G + F \end{vmatrix}_i$$

The matrices D_1 and F are given in equations (E.6) and (E.7). Here because of symmetry the coupling matrices H_{21} and H_{31} are null matrices, since the coupling effect due to one cantilever at one side is nullified by the cantilever on the other side (figure A.1).

b) Asymmetric section ($m=2$)

The equations of equilibrium at node i are (figure A.2)

$$M_i = M_{1i} - M_{2i} \tag{A.4}$$

$$F_i = F_{1i} - P_{2i}$$

$$P_i = P_{1i} + F_{2i}$$

and the transfer matrix $[H_2]_i$ is

$$[H_2]_i = \begin{vmatrix} H_{12} & H_{22} \\ H_{32} & H_{42} \end{vmatrix} = \begin{vmatrix} B + D_2 & C_2 \\ E_2 & G + 1/2 F \end{vmatrix}$$

matrices C_2 , D_2 and E_2 are given in equations (E.8), (E.9) and (E.10).

c) Antisymmetric section ($m=3$)

A section of this type can be considered to be composed of two sections of asymmetric type where one is rotated 180° with respect to the other about an axis along the length of the section (figure A.3). The transfer matrix for part I ($[H_3]_i^I$) is the same as that of the asymmetric section:

$$[H_3]_i^I = [H_2]_i$$

and that for part II ($[H_3]_i^{II}$), using the equations of equilibrium

$$\begin{aligned} M_i &= M_{1i} - M_{2i} \\ F_i &= F_{1i} + P_{2i} \\ P_i &= P_{1i} - F_{2i} \end{aligned} \tag{A.5}$$

is

$$[H_3]_i^{\text{II}} = \left[\begin{array}{c|c} B + D_2 & -C_2 \\ \hline -E_2 & G + 1/2 F \end{array} \right]$$

Now, the transfer matrix for the whole section is the product of the two above, i.e.,

$$[H_3]_i = [H_3]_i^{\text{I}} [H_3]_i^{\text{II}} \quad (\text{A.6})$$

APPENDIX B

Impedance Matrix at the n'th node

In the semi-infinite uniform beam extension of the main beam, the solution for the amplitudes of the time dependent part of the bending and axial modes of vibration traveling to the right are (figure B.1):

$$\begin{aligned}v(x) &= B_1 \exp(-\beta x) + B_2 \exp(-j\beta x) \\u(x) &= B_3 \exp(-j\gamma x)\end{aligned}$$

The above solutions are completely determined by the three displacement boundary conditions (v_n , θ_n/β and u_n) at the n'th node. We obtain the components of the force vector ($M_n/EI\beta^2$, $-F_n/EI\beta^3$ and $P_n/\gamma EA$) at the n'th node by differentiating the solutions and using the constitutive relations

$$M_n/EI\beta^2 = v''(x)\Big|_{x=0}, \quad -F_n/EI\beta^3 = v'''(x)\Big|_{x=0}$$

$$\text{and} \quad P_n/\gamma EA = u'(x)\Big|_{x=0}$$

Since $N_n = Q_n^+ W_n$

the impedance matrix, Q_n^+ , at the n'th node is

$$Q_n^+ = \begin{vmatrix} -j & -(1+j) & 0 \\ -(1-j) & j & 0 \\ 0 & 0 & j \end{vmatrix} \quad (\text{B.1})$$

APPENDIX C

C.1 Transfer Impedance Matrix $[R_{on}^+]_m$

From equation (2.3.2):

$$\begin{Bmatrix} W_{i-1} \\ \text{---} \\ N_{i-1} \end{Bmatrix} = [K_m]_i \begin{Bmatrix} W_i \\ \text{---} \\ N_i \end{Bmatrix} \quad (\text{C.1})$$

where $[K_m]_i = [\hat{H}_m]_i^{-1}$

$[\hat{H}_m]_i$ is the matrix $[H_m]_i$ rearranged in the same way as \hat{Z}_i . Since $[H_m(\alpha)]_i^{-1}$ is the transfer matrix from the i 'th node to the $(i-1)$ 'th node, it is most easily found by changing the sign of x which makes α_1 and α_2 negative in the equations (E.1), (E.2), (E.6), (E.7), (E.9) and (E.10) of appendix E.

After partitioning the matrix $[K_m]_i$, into four parts

$$[K_m]_i = \begin{vmatrix} \{K_{m1}\}_i & | & \{K_{m2}\}_i \\ \text{---} & | & \text{---} \\ \{K_{m3}\}_i & | & \{K_{m4}\}_i \end{vmatrix}$$

we have
$$W_{i-1} = \{K_{m1}\}_i W_i + \{K_{m2}\}_i N_i \quad (\text{C.2})$$

$$N_{i-1} = \{K_{m3}\}_i W_i + \{K_{m4}\}_i N_i$$

Equations (C.2) are valid for any section i . Starting with the n 'th section, we have:

$$W_{n-1} = \{K_{m1}\}_n W_n + \{K_{m2}\}_n N_n$$

$$N_{n-1} = \{K_{m3}\}_n W_n + \{K_{m4}\}_n N_n$$

Substituting for N_n from equation (B.1) and inverting the first equation to find W_n

$$W_n = [\{K_{m1}\}_n + \{K_{m2}\}_n Q_n^+]^{-1} W_{n-1} \quad (C.3)$$

then
$$N_{n-1} = Q_{n-1}^+ W_{n-1}$$

where
$$Q_{n-1}^+ = [\{K_{m3}\}_n + \{K_{m4}\}_n Q_n^+] [\{K_{m1}\}_n + \{K_{m2}\}_n Q_n^+]^{-1}$$

is the impedance matrix at $(n-1)$ 'th node and can be determined since all the terms on the right hand side are known.

In a similar fashion for any node i we find that

$$Q_i^+ = [\{K_{m3}\}_{i+1} + \{K_{m4}\}_{i+1} Q_{i+1}^+] [\{K_{m1}\}_{i+1} + \{K_{m2}\}_{i+1} Q_{i+1}^+]^{-1} \quad (C.4)$$

and
$$W_i = [\{K_{m1}\}_i + \{K_{m2}\}_i Q_i^+]^{-1} W_{i-1}$$

Applying equation (C.4) successively, we find W_n in terms of W_0 . Then we find the force vector at the n'th node (the point of measurement) in terms of the displacement vector at the 0'th node (the point of impact) from equation (B.1)

$$N_n = Q_n^+ W_n = [R_{0n}^+]_m W_0$$

where

$$[R_{0n}^+]_m = Q_n^+ \left[\{K_{m1}\}_n + \{K_{m2}\}_n Q_n^+ \right]^{-1} \left[\{K_{m1}\}_{n-1} + \{K_{m2}\}_{n-1} Q_{n-1}^+ \right]^{-1} \dots \dots \dots \left[\{K_{m1}\}_2 + \{K_{m2}\}_2 Q_2^+ \right]^{-1} \left[\{K_{m1}\}_1 + \{K_{m2}\}_1 Q_1^+ \right]^{-1} \quad (C.5)$$

In our case, all the sections are identical and all of the K_m matrices are equal.

C.2 An alternative method of computing matrix $[R_{0n}^+]_m$

Instead of having to invert the matrices at each node as shown in equation (C.5) we could successively substitute from the left hand side of equation (C.1) into the right side at each node. This would give the forces and displacements at the 0'th node in terms of those at the n'th node:

$$\begin{Bmatrix} W_0 \\ \dots \\ N_0 \end{Bmatrix} = [K_m]_1 [K_m]_2 \dots \dots [K_m]_{n-1} [K_m]_n \begin{Bmatrix} W_n \\ \dots \\ N_n \end{Bmatrix}$$

$$= T_m \begin{Bmatrix} W_n \\ \text{---} \\ N_n \end{Bmatrix} \quad (\text{C.6})$$

We can now partition T_m to get

$$T_m = \begin{vmatrix} T_{m1} & T_{m2} \\ \text{---} & \text{---} \\ T_{m3} & T_{m4} \end{vmatrix}$$

and
$$W_o = T_{m1} W_n + T_{m2} N_n = (T_{m1} + T_{m2} Q_n^+) W_n$$

so that
$$W_n = (T_{m1} + T_{m2} Q_n^+)^{-1} W_o \quad (\text{C.7})$$

which is only one inversion. Unfortunately, at large α_2 and α_4 , the hyperbolic terms in matrices G , C_2 and F , appendix E, are very large and almost equal. As a result the elements of $(T_{m1} + T_{m2} Q_n^+)$ are the small differences of large numbers and the matrix is very ill-conditioned. Even though this is only a 2x2 matrix for the symmetric case we lost more than 10 digits for three multiplications at frequencies as low as 3000 Hz. As a result, the successive inversion method was used for all cantilevers. Even so, some care must be taken since we lose 6 digits at 10000 Hz.

APPENDIX D

Derivation of the Matrix S

The equations for the incident waves traveling towards the right are

$$v_I = V_1 \exp [j(\omega t - \beta x)] \tag{D.1}$$

$$u_I = U_1 \exp [j(\omega t - \gamma x)]$$

where u and v are the deflection in the positive direction of x and y respectively (figure 2.5.2).

For the reflected wave traveling towards the left

$$v_R = V_2 \exp [j(\omega t + \beta x)] + V_3 \exp [\beta x + j\omega t] \tag{D.2}$$

$$u_R = U_2 \exp [j(\omega t + \gamma x)]$$

At node zero the transmitted displacements are v_o , θ_o and u_o which are related to the internal forces at the node by

$$N_o = Q_o^+ W_o$$

Equation (2.6.4) written for its all components is

$$\begin{aligned}
V_1 &= V_2 + V_3 + V_0 \\
-jV_1 &= jV_2 + V_3 + \theta_0 / \beta \\
U_1 &= U_2 + U_0
\end{aligned}
\tag{D.3}$$

and that for the equations of equilibrium,

$$\begin{aligned}
M_I / EI \beta^2 &= M_R / EI \beta^2 + M_0 / EI \beta^2 \\
F_I / EI \beta^3 &= F_R / EI \beta^3 + F_0 / EI \beta^3 \\
P_I / \gamma EA &= P_R / \gamma EA + P_0 / \gamma EA
\end{aligned}
\tag{D.4}$$

The relations between the components of N_k and those of displacement W_k are

$$N_I = \left\{ \begin{array}{l} M_I / EI \beta^2 = -V_1 \\ -F_I / EI \beta^3 = -jV_1 \\ P_I / \gamma EA = -jU_1 \end{array} \right\} ; \quad N_R = \left\{ \begin{array}{l} M_R / EI \beta^2 = -V_2 + V_3 \\ -F_R / EI \beta^3 = -jV_2 + V_3 \\ P_R / \gamma EA = jU_2 \end{array} \right\}
\tag{D.5}$$

and

$$N_0 = \left\{ \begin{array}{l} M_0 / EI \beta^2 \\ -F_0 / EI \beta^3 \\ P_0 / \gamma EA \end{array} \right\} = Q_0^+ \left\{ \begin{array}{l} v_0 \\ \theta_0 / \beta \\ u_0 \end{array} \right\} = Q_0^+ W_0$$

We now solve for V_2 and V_3 in terms of V_1 and v_0 and U_2 in terms of U_1 and u_0 from equations (D.3). We then use these to find the elements of N_k in terms of V_1, v_0, U_1 and u_0 in equations

(D.5). We substitute for V_I and U_I in terms of M_I , F_I and P_I from equations (D.5) and finally a set of linear equations for M_I , F_I and P_I in terms of v , θ_0 and u ,

$$N_I = S W_0$$

where

$$S = \begin{vmatrix} \left(\frac{1+j}{4}\right) \{Q_0^+(1,1) + j\} & \left(\frac{1+j}{4}\right) \{Q_0^+(1,2) - (1+j)\} & \left(\frac{1+j}{2}\right) \{Q_0^+(1,3)\} \\ \left(\frac{1-j}{4}\right) \{Q_0^+(2,1) - 1+j\} & \left(\frac{1-j}{4}\right) \{Q_0^+(2,2) - j\} & \left(\frac{1-j}{4}\right) Q_0^+(2,3) \\ \frac{1}{2} Q_0^+(3,1) & \frac{1}{2} Q_0^+(3,2) & \frac{1}{2} \{Q_0^+(3,3) - j\} \end{vmatrix} \quad (D.6)$$

APPENDIX E

Differentiating equation (2.2.4) we have

$$P = EA u' = EA \gamma [-E_1 \cos \gamma x + E_2 \sin \gamma x]$$

$$\theta = v' = A_1 \beta \sinh \beta x + A_2 \beta \cosh \beta x - A_3 \beta \sin \beta x + A_4 \beta \cos \beta x$$

$$M = EI v'' = EI \beta^2 [A_1 \cosh \beta x + A_2 \sinh \beta x - A_3 \cos \beta x - A_4 \sin \beta x]$$

$$F = -EI v''' = -EI \beta^3 [A_1 \sinh \beta x + A_2 \cosh \beta x + A_3 \sin \beta x - A_4 \cos \beta x]$$

Substituting $x=0$, solving for E_1, E_2, A_1, A_2, A_3 and A_4 in terms of u, v and their derivatives and then solving for the elements of Z_i at $x = L$, we get:

$$Z_{1i} = B Z_{1(i-1)}$$

$$Z_{2i} = G Z_{2(i-1)}$$

where

$$B = \begin{vmatrix} \cos \alpha_1 & \sin \alpha_1 \\ -\sin \alpha_1 & \cos \alpha_1 \end{vmatrix} \quad (E.1)$$

$$a_1 = \cosh \alpha_2 + \cos \alpha_2$$

$$a_2 = \sinh \alpha_2 + \sin \alpha_2$$

$$a_3 = \cosh \alpha_2 - \cos \alpha_2$$

$$a_4 = \sinh \alpha_2 - \sin \alpha_2$$

$$G = \frac{1}{2} \begin{vmatrix} a_1 & a_2 & a_3 & a_4 \\ a_4 & a_1 & a_2 & a_3 \\ a_3 & a_4 & a_1 & a_2 \\ a_2 & a_3 & a_4 & a_1 \end{vmatrix} \quad (E.2)$$

$$\text{and } \alpha_1 = \frac{\omega L}{c_r} \quad , \quad \alpha_2 = \beta L \quad , \quad \beta^4 = \frac{\rho A \omega^2}{EI}$$

If we now make the change to local coordinates for the cantilevers, and put in the boundary conditions for the cantilever

$$P = F = M = 0 \text{ at } x_2 = h \quad (\text{figure 2.3.1})$$

$$\text{we get } P_{2i} / \gamma EA = \tan \alpha_3 u_{1i} \quad (\text{E.3})$$

$$\begin{Bmatrix} M_{2i} / EI \beta^2 \\ -F_{2i} / EI \beta^3 \end{Bmatrix} = A \begin{Bmatrix} u_{1i} \\ \theta_{1i} / \beta \end{Bmatrix} \quad (\text{E.4})$$

$$A = \frac{1}{\Delta} \begin{vmatrix} \sinh \alpha_4 \sin \alpha_4 & \cosh \alpha_4 \sin \alpha_4 - \sinh \alpha_4 \cos \alpha_4 \\ -(\cosh \alpha_4 \sin \alpha_4 + \sinh \alpha_4 \cos \alpha_4) & -(\sinh \alpha_4 \sin \alpha_4) \end{vmatrix}$$

$$\alpha_3 = \frac{\omega h}{c_r} \quad , \quad \alpha_4 = \beta h \quad , \quad \Delta = (1 + \cosh \alpha_4 \cos \alpha_4)$$

a) Symmetric section ($m = 1$)

Substituting from equations (E.1), (E.2), (E.3) and (E.4) into equation (A.3) we finally get that

$$[H_1]_i = \left| \begin{array}{c|c} B + D_1 & 0 \\ \hline 0 & G + F \end{array} \right| \quad (E.5)$$

where

$$D_1 = -\frac{2\omega}{\beta c_r} \frac{1}{\Delta \cdot c} \left| \begin{array}{c|c} 0 & 0 \\ \hline -\cos \alpha_1 & -\sin \alpha_1 \end{array} \right| \quad (E.6)$$

$$F = \left| \begin{array}{cccc} 0 & 0 & 0 & 0 \\ 0 & 0 & 0 & 0 \\ a \cdot a_4 & a \cdot a_1 & a \cdot a_2 & a \cdot a_3 \\ b \cdot a_1 & b \cdot a_2 & b \cdot a_3 & b \cdot a_4 \end{array} \right| \quad (E.7)$$

$$C = (\cosh \alpha_4 \sin \alpha_4 + \sinh \alpha_4 \cos \alpha_4)$$

$$a = -\frac{\cosh \alpha_4 \sin \alpha_4 - \sinh \alpha_4 \cos \alpha_4}{1 + \cosh \alpha_4 \cos \alpha_4}, \quad b = \frac{\beta c_r \tan \alpha_3}{\omega}$$

b) Asymmetric section (m = 2)

Substituting equations (E.1), (E.2), (E.3) and (E.4) into equation (A.4) we get

$$[H_2]_i = \left| \begin{array}{c|c} B + D_2 & C_2 \\ \hline E_2 & G + \frac{1}{2} F \end{array} \right| \quad (E.8)$$

where

$$D_2 = \frac{\omega}{\beta c_r} \cdot \frac{1}{2\Delta} \begin{vmatrix} 0 & 0 \\ -c & -c \end{vmatrix}$$

$$C_2 = \frac{\omega}{\beta c_r} \cdot \frac{1}{2\Delta} \begin{vmatrix} 0 & 0 & 0 & 0 \\ a_4 & a_1 & a_2 & a_3 \end{vmatrix} \quad (\text{E.9})$$

$$E = \begin{vmatrix} 0 & 0 \\ 0 & 0 \\ d \cos \alpha_1 & d \sin \alpha_1 \\ 0 & 0 \end{vmatrix} \quad (\text{E.10})$$

$$d = (\sinh \alpha_u \sin \alpha_u) / \Delta$$

c) Antisymmetric section (m = 3)

After substituting equations (E.1), (E.2), (E.3) and (E.4) into equation (A.5), the transfer matrix for part II is obtained as

$$[H_3]_i^{\text{II}} = \begin{vmatrix} B + D_2 & -C_2 \\ -E_2 & G + \frac{1}{2}F \end{vmatrix} \quad (\text{E.11})$$

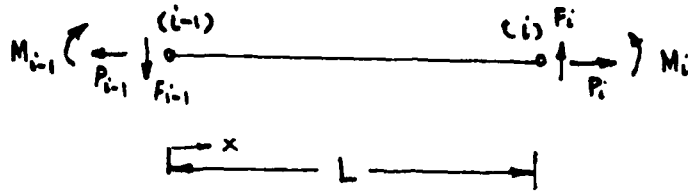
REFERENCES

1. Brillouin, L. "Wave Propagation in Periodic Structures", Dover Publications , 1953.
2. Elachi, C. " Waves in Active and Passive Periodic Structure: A Review" , IEEE Proc., 64(12) , Dec 1976.
3. Cremer, L.; Heckl, M. and Ungar, E. E. "Structure-Borne Sound", Springer-Verlag, 1973, Chapter V, Section 5.
4. Abdul-Rahman, A. Y. A. and Petyt, M. "Free and Forced Wave Propagation in Two-dimensional Periodic Systems Using Matrix Techniques" , Recent Advances in Structural Dynamics: Vol I pp 361-373 (Inst. of Sound and Vibration Research, Univ. of Southampton, UK, 1980)
5. Mead, D. J. "A general theory of harmonic wave propagation in linear periodic systems with multiple coupling", Journal of Sound and Vibration, 1973, 27(2), pp 235-260.
6. Sengupta, G. "Vibration of Periodic Structures", Shock and Vibration Digest, March 1980, pp17-31.

7. Gruzin, V. V.; Kandidov, V. P. and Shmal'gauzen, V. I.
"Filtering of Elastic Waves in a Bar with Ribs"
IZY AN SSSR. Mekhanika Tverdogo Tela, Vol 12,
No 4, pp 180-184, 1977, Trans. Allerton Press
1977.

8. Plunkett, R. and Roy, A. "Wave Attenuation in Damped
Periodic Structures", Interim Technical Report
N00014-82-K - 0591 , ONR , 12 July 1983.

Beam Element



Cantilever Element

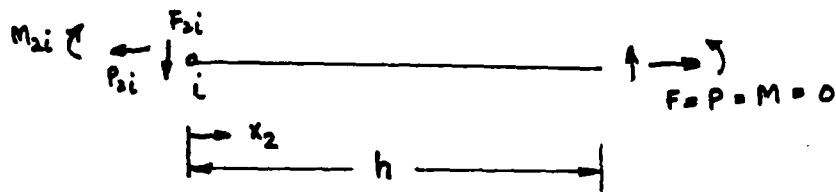
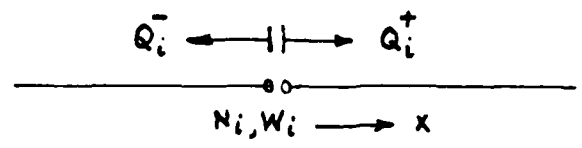


Figure 2.3.1

Impedance Matrix at a node i



node i

Figure 2.6.1

Incident, Reflected and Transmitted wave at node 0

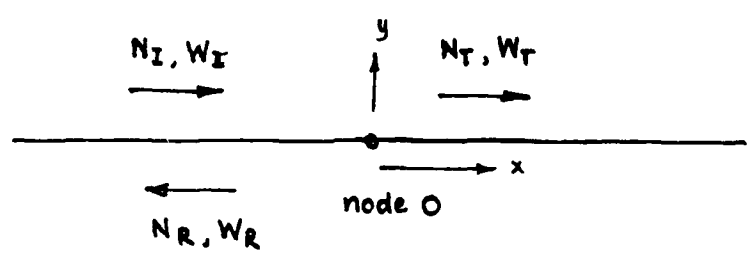


Figure 2.5.2

Schematic diagram of the Instrumentation

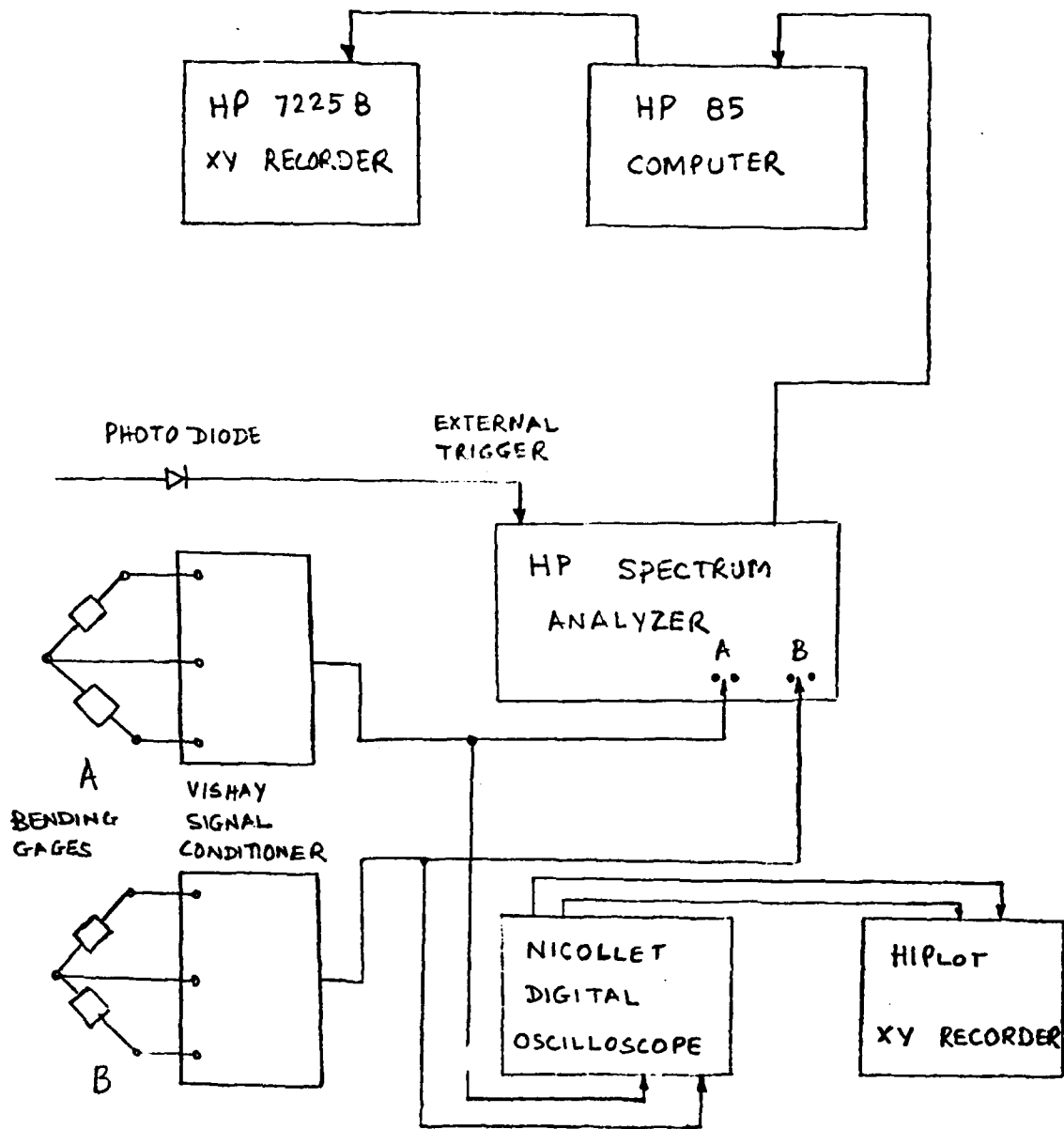
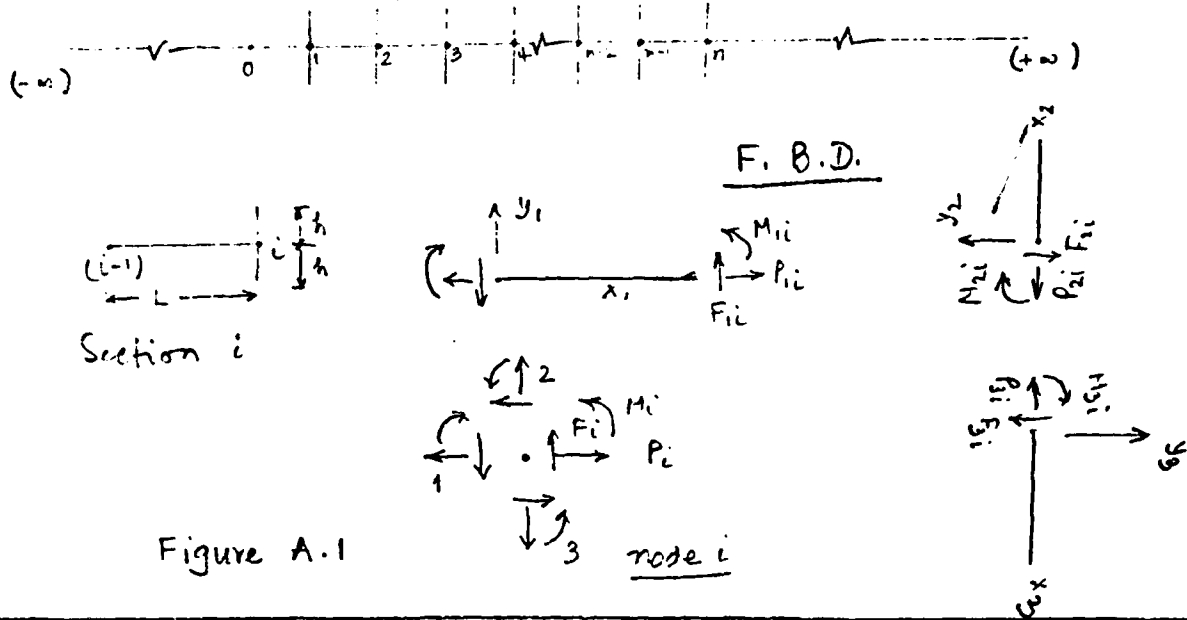


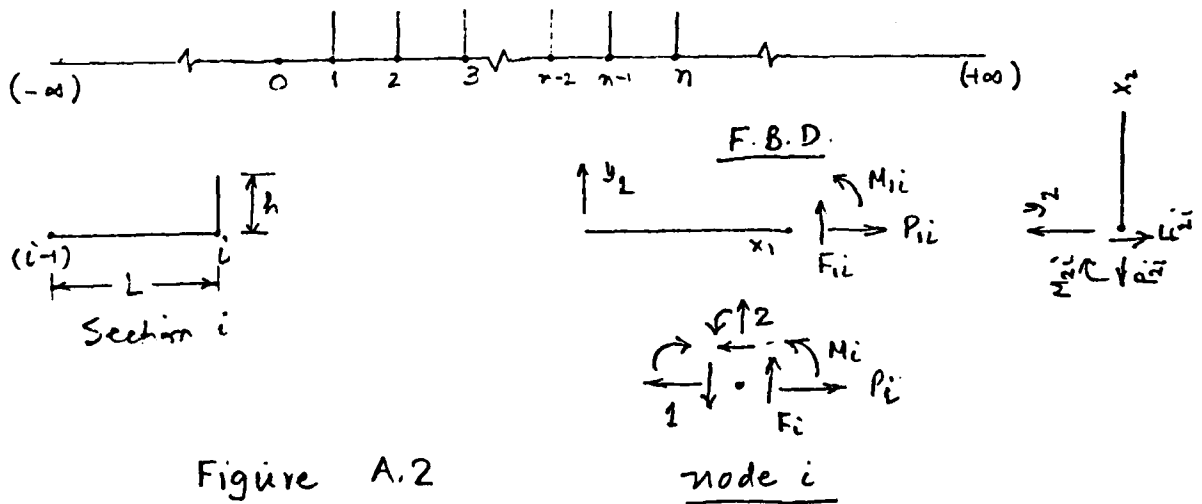
Figure 3.1.1

Geometry of the periodic beam and Free Body Diagram (F.B.D.)

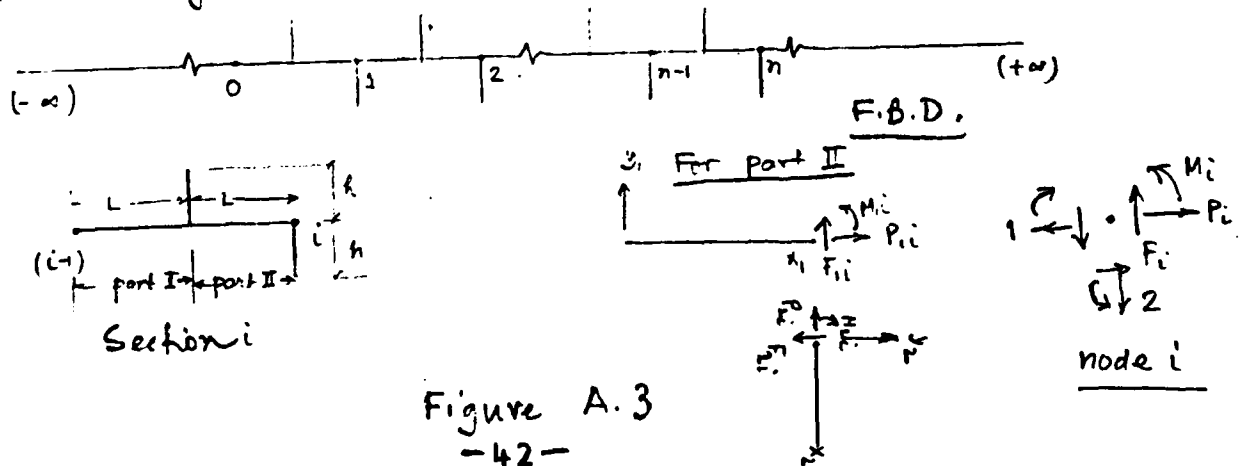
1) Symmetric periodic beam



2) Asymmetric periodic beam



3) Anti-symmetric periodic beam.



Impedance Matrix of semi-infinite uniform
beam at node n

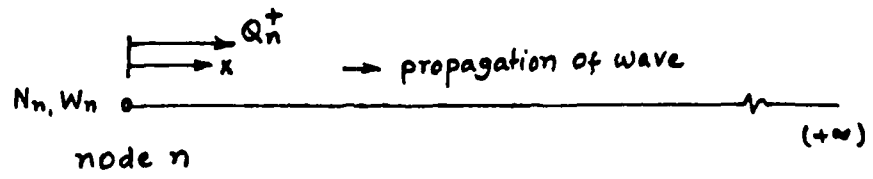
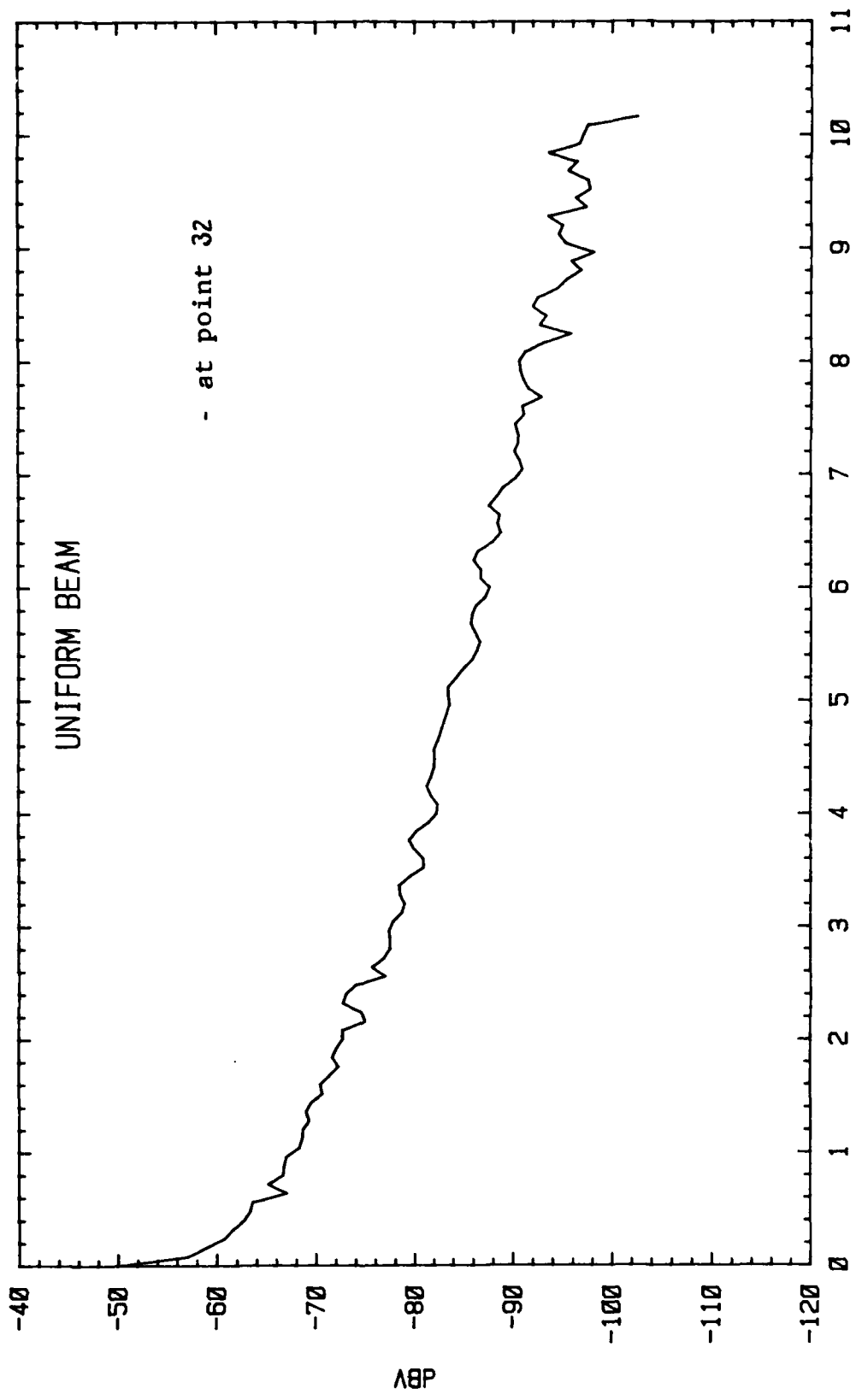


Figure B.1



FREQUENCY (kHz)

Figure 3.3.1

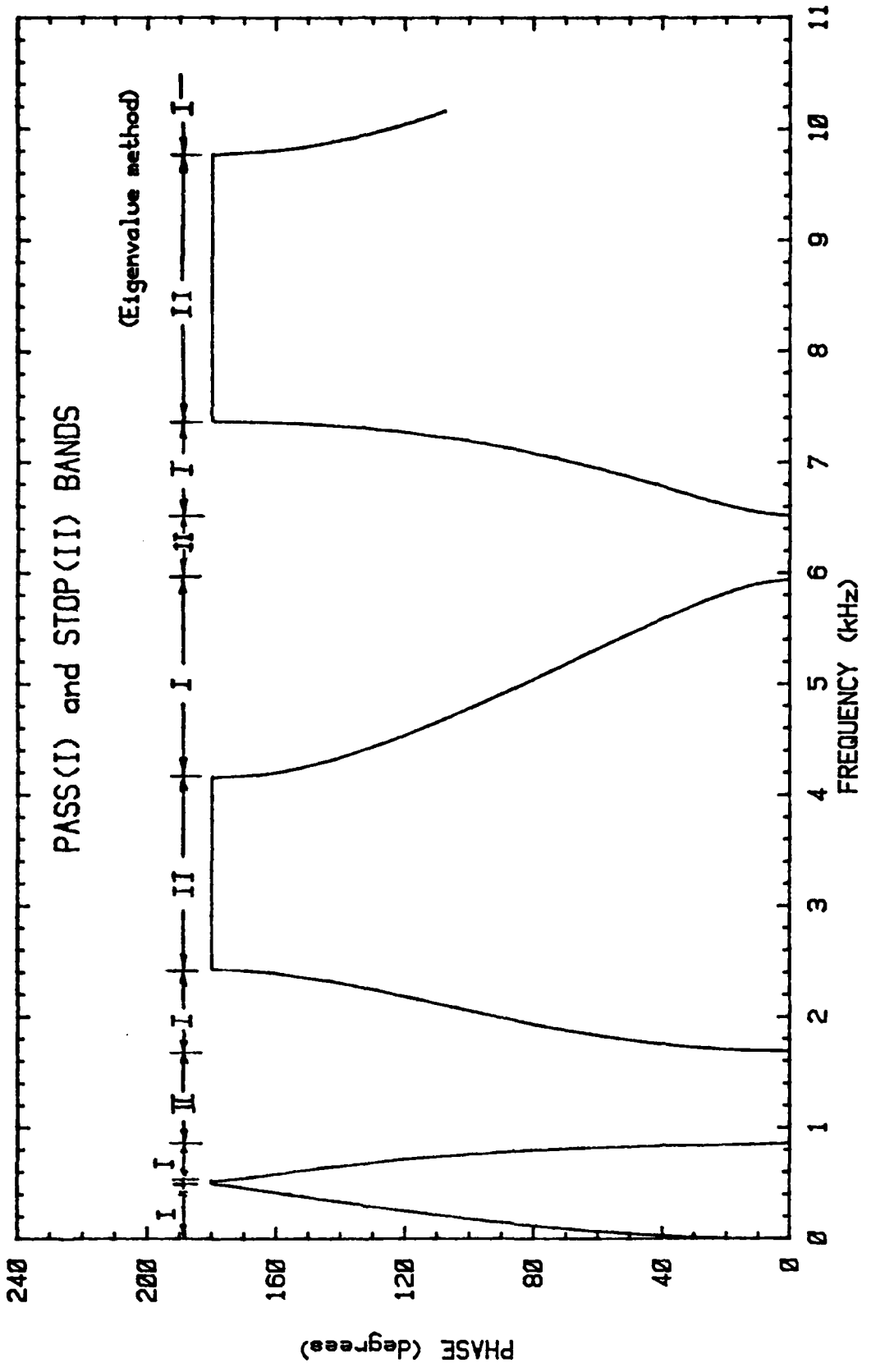


Figure 4.1.1

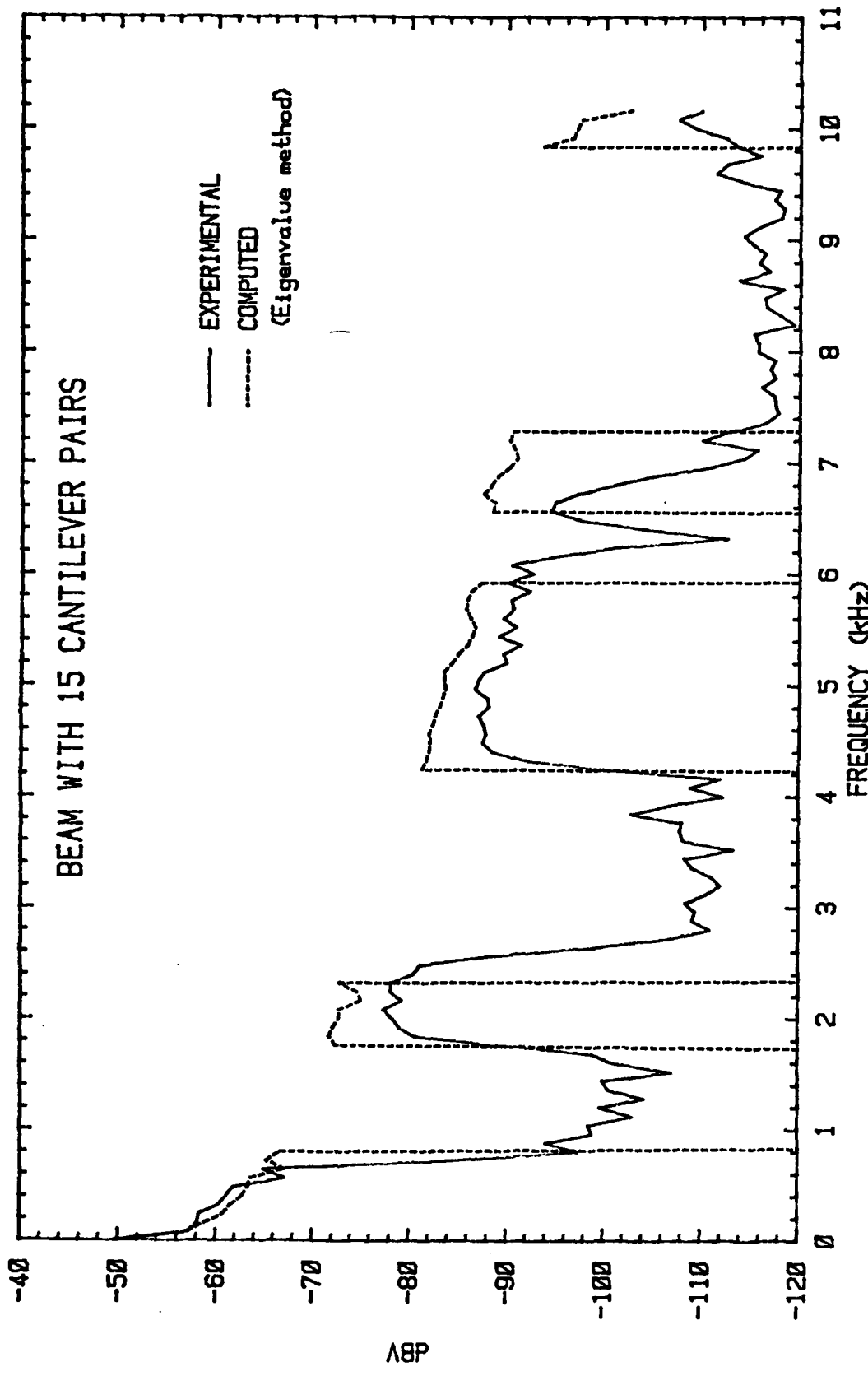


Figure 4.1.2

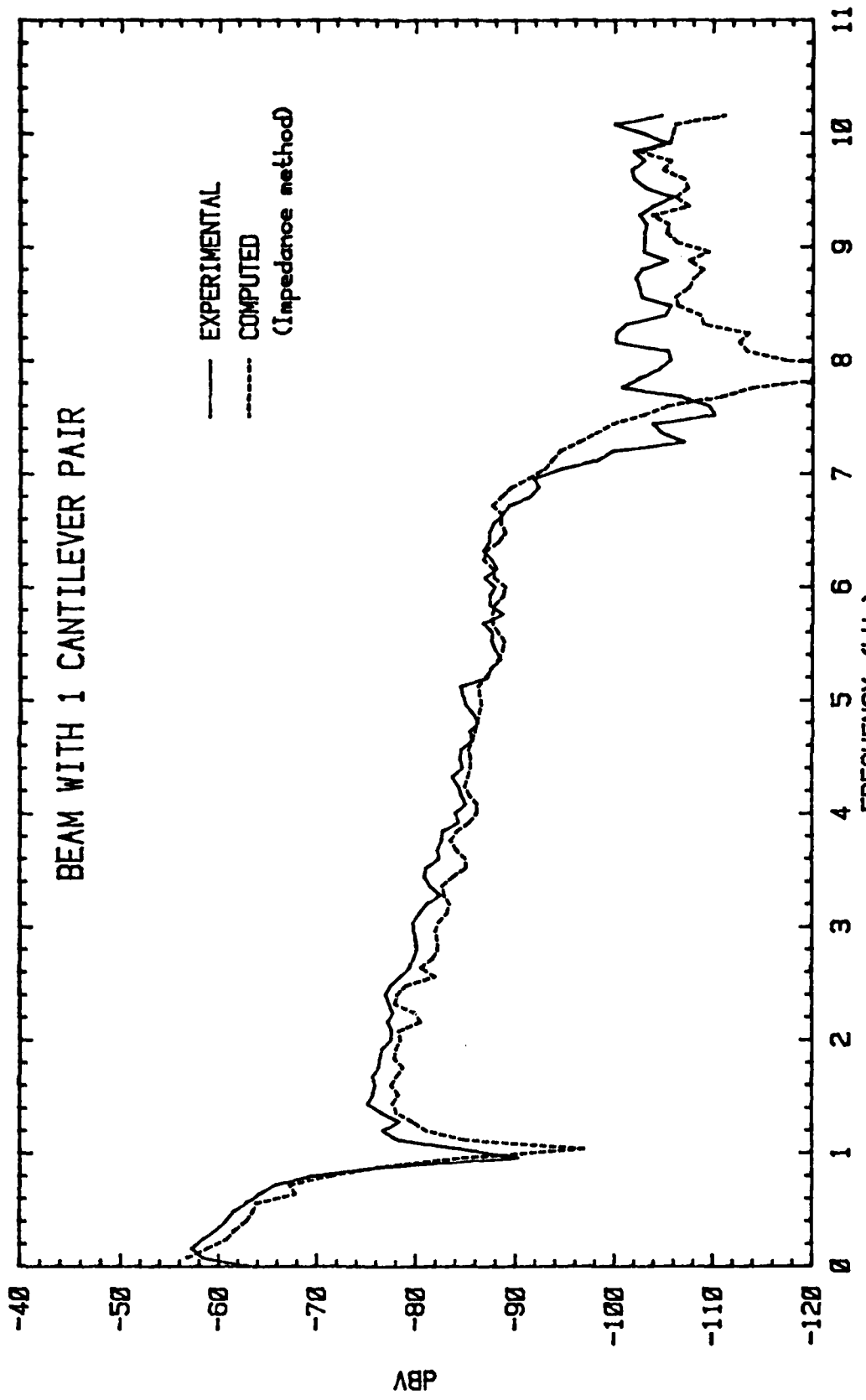


Figure 4.2.2a

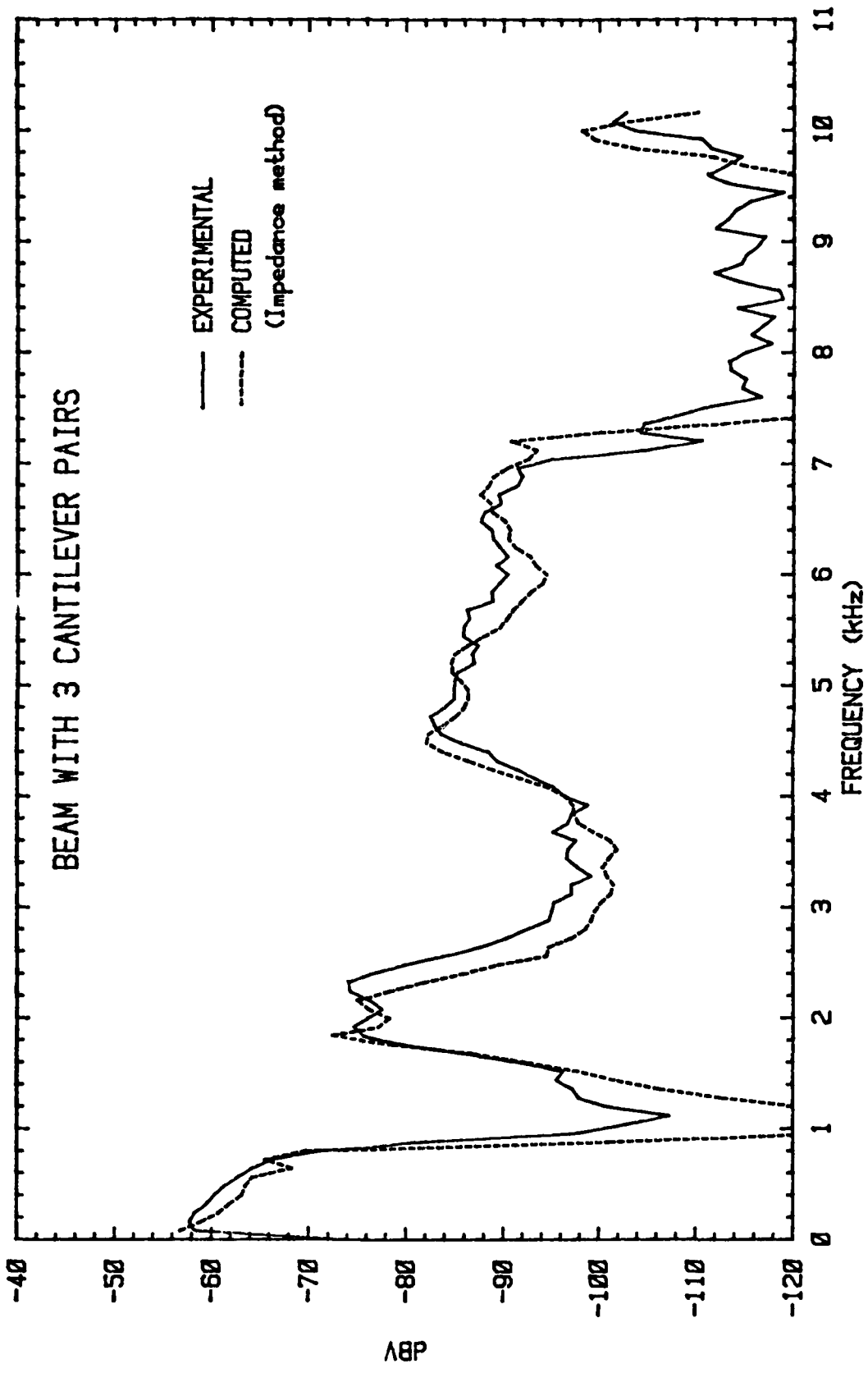


Figure 4.2.2b

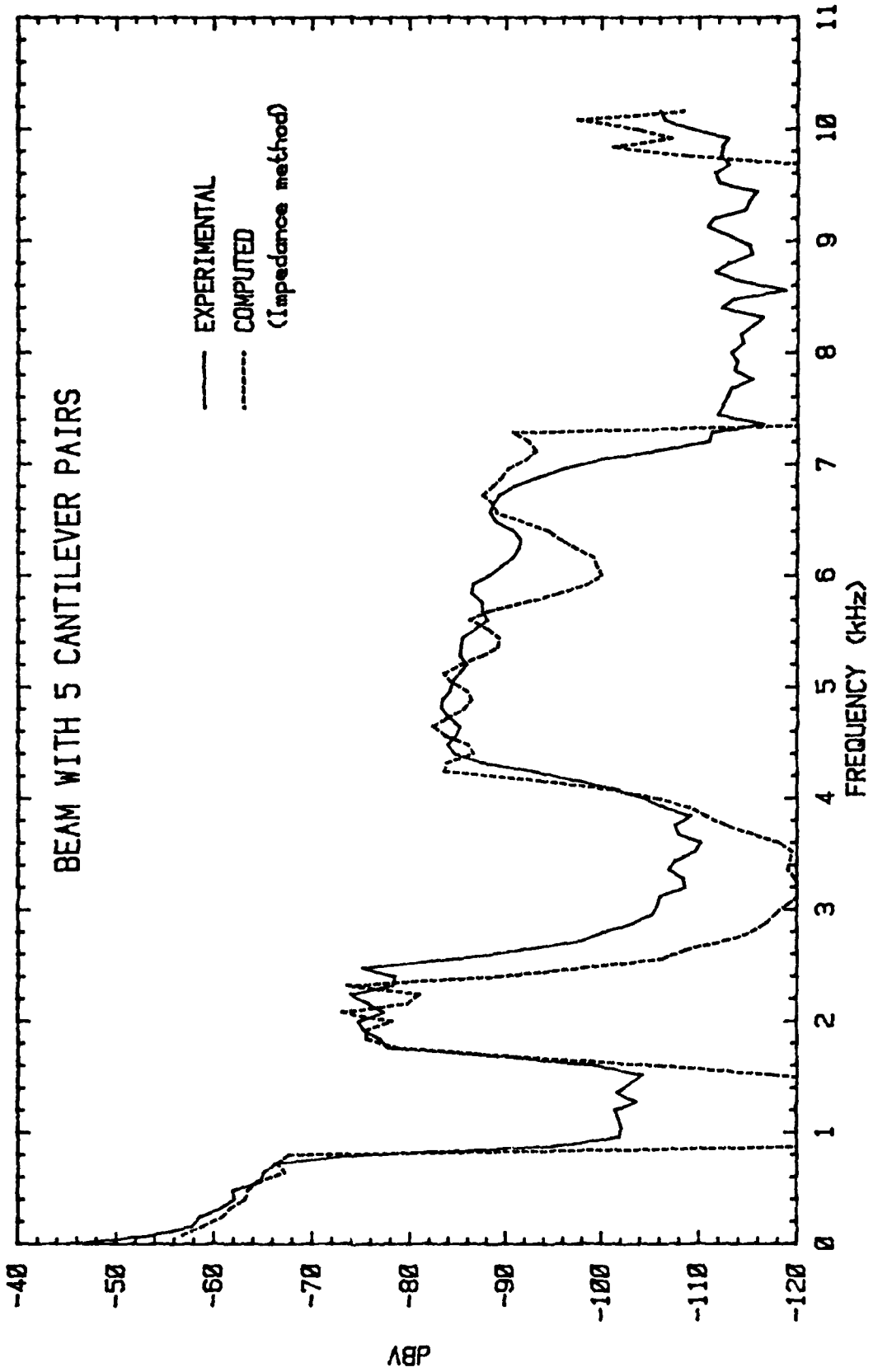


Figure 4.2.2c

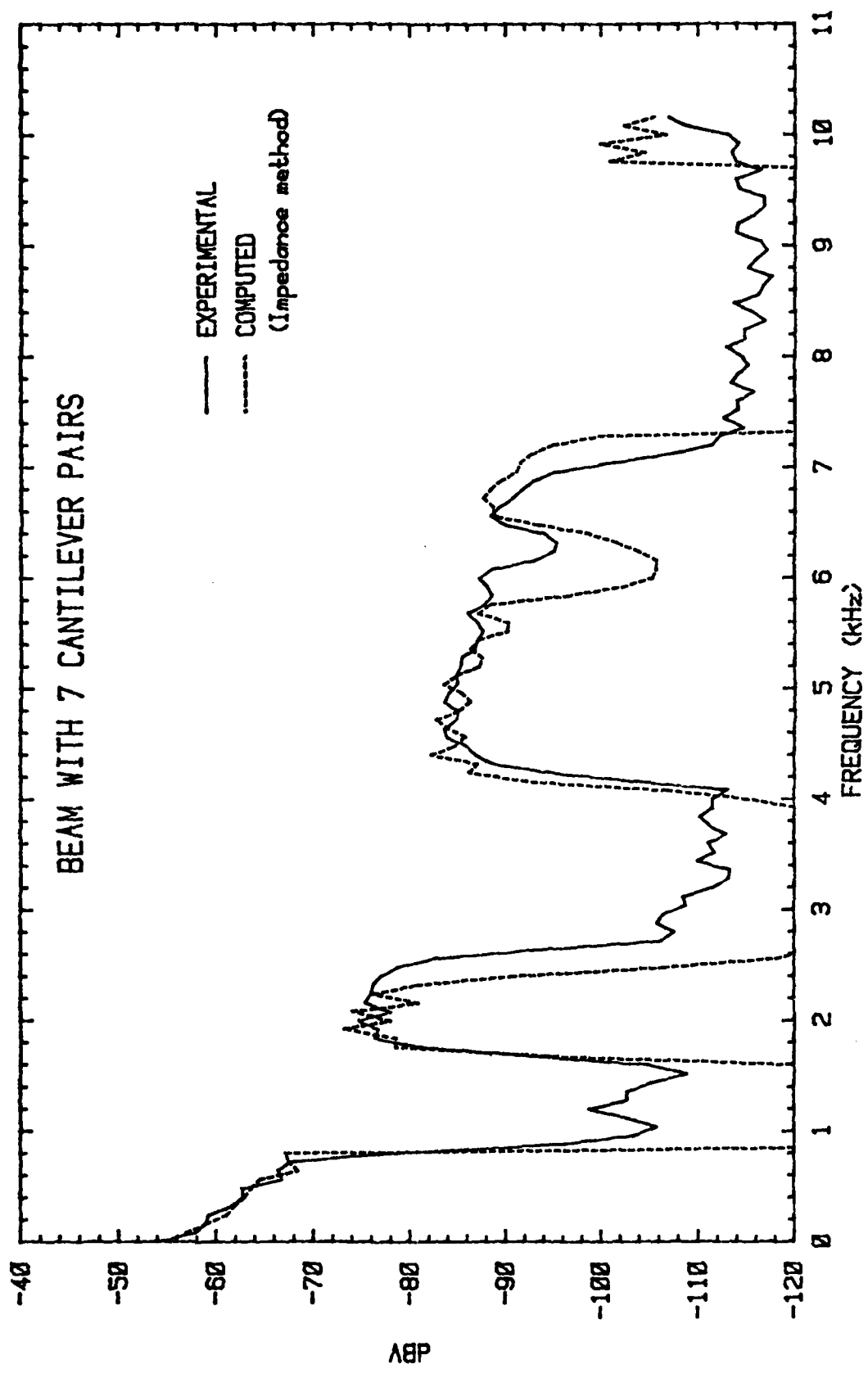


Figure 4.2.2d

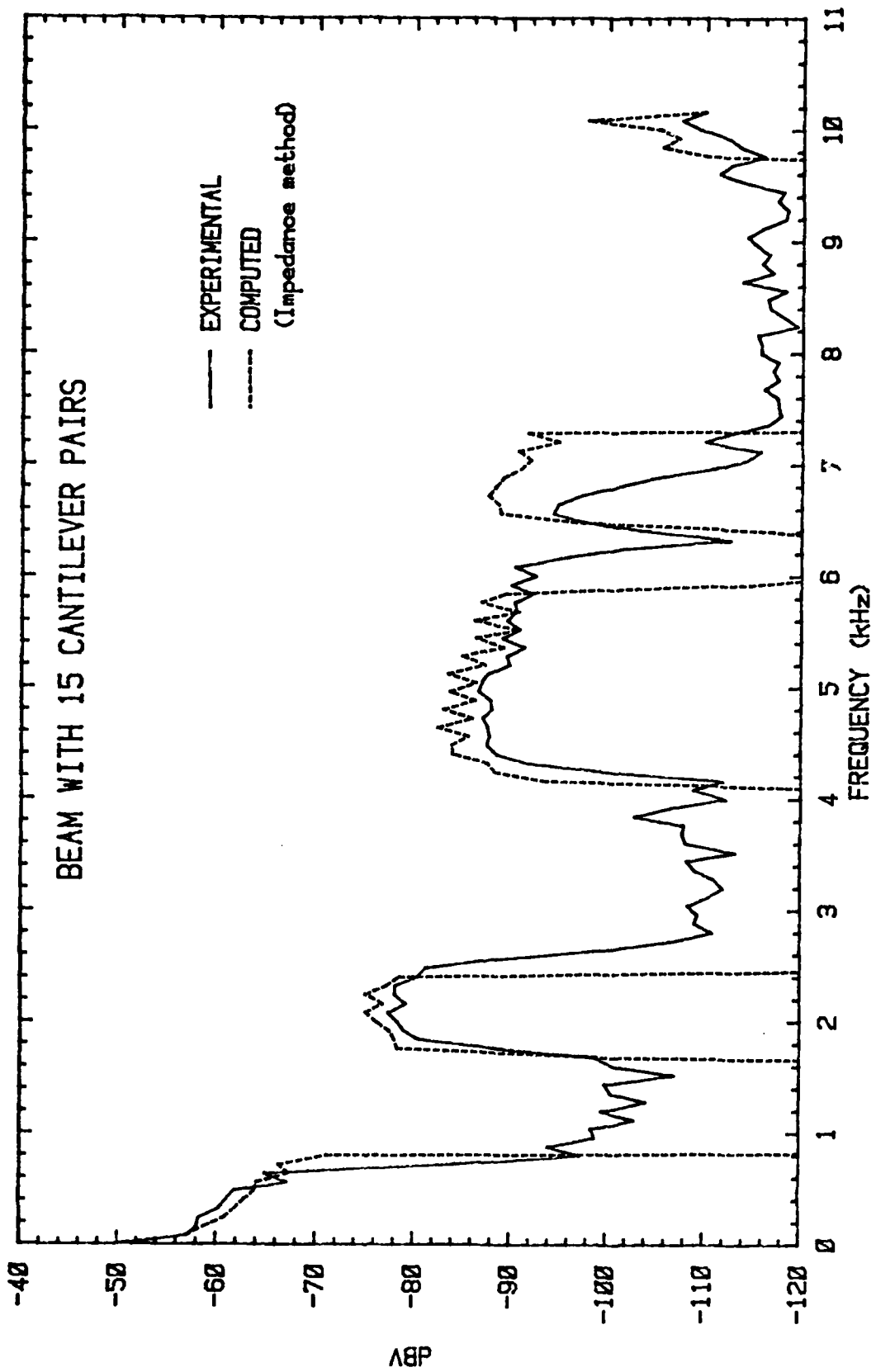


Figure 4.2.2e

END

FILMED

4-84

DTIC